Optical properties of Si-doped InN grown on sapphire (0001)

T. Inushima*
Department of Electronics, Tokai University, Kitakaname, Hiratsuka 259-1292, Japan

M. Higashiwaki and T. Matsui
Communications Research Laboratory, Nukui-Kita, Koganei, Tokyo 184-8795, Japan

(Received 26 March 2003; revised manuscript received 24 June 2003; published 4 December 2003)

The carrier concentration dependence of the interaction between free carriers and longitudinal optical (LO) phonons of InN is studied by Raman scattering and Fourier transform infrared measurements. InN is grown on a sapphire (0001) surface by plasma-assisted molecular beam epitaxy. The carrier concentration is varied from 1.8×10^{18} to 1.5×10^{19} cm^{-3} by Si doping. The infrared reflection spectra, to which the vibration in the *a-b* plane contributes, reveal a linear coupling between the $E_1(LO)$ phonon and the plasma oscillation of the free carriers. From the plasma frequency the electron effective mass is estimated to be $m^*_{e\perp}=0.085m_0$ for the intrinsic InN. The Raman spectra, to which the vibration along the *c* axis contributes, reveal that the $A_1(LO)$ phonon and free carriers couple nonlinearly, where a Fano interference between the zone-center LO phonon and the quasicontinuum electronic state along the *c* axis is prominent. With these results, the anisotropic electronic structure of InN is discussed.

DOI: 10.1103/PhysRevB.68.235204 PACS number(s): 78.20.−e, 78.30.Fs, 78.40.Fy

I. INTRODUCTION

Among III-nitride semiconductors, InN is a key material for optical and high electron mobility device applications.[1] In most of the reports so far InN has been grown on a sapphire (0001) substrate and it is a degenerate *n*-type semiconductor with a carrier concentration higher than 10^{18} cm^{-3}. Its crystal structure is hexagonal with the *c* axis parallel to the substrate *c* axis. The band gap energy was reported in earlier studies to be 1.9 eV.[2,3] With the recent development of a molecular beam epitaxy (MBE) growth method of InN, however, the crystal quality has been greatly improved, which has enabled us to reveal that the band gap energy of InN should be much smaller than 1.9 eV.[4] Recently Davydov *et al*. observed strong luminescence of InN at 0.9 eV, from which they concluded that the band gap energy of InN was 0.7 eV.[5,6] This value, however, poses several problems to be solved. One is that it is contradictory to the bond and band criterion that InN should have a wider band gap energy than InP (1.42 eV).[7] Another is the high carrier concentration of InN. In spite of the great effort to grow high quality InN, there has been no report of semiconducting InN. Moreover, one of the authors (T.I.) found that some InN became superconductors below 3.4 K, and that it showed an anisotropic superconductivity at 1.5 K.[8] From the angle dependence of the magnetoresistance between the applied field and the crystal *c* axis, it was concluded that the electronic structure of InN was anisotropic.[9]

As for understanding the phonon structure of InN, many optical measurements have been done.[10,11] InN has four atoms per unit cell and belongs to the C^4_{6v} space group, from which one A_1, one E_1, two E_2 and two B_1 optical phonons are predicted at the Γ point of the Brillouin zone. Among them, A_1 and E_1 phonons are both Raman- and infrared-active polar modes, E_2 is a Raman-active nonpolar mode, and B_1 is a silent mode. When free electrons exist in polar semiconductors, the plasma oscillation of the free carriers couples strongly with the longitudinal optical (LO) phonons via their macroscopic longitudinal electric field (Fröhlich interaction) and forms a plasmon–LO- phonon coupled mode. In an earlier study of InN which contains a carrier concentration of the order of 10^{19} cm^{-3}, InN shows a strong plasma reflection in the infrared reflection spectra in the *a-b* plane,[10,12] and, from the plasma frequency vs free carrier concentration relation, it was reported that the electron effective mass depends strongly on the free electron concentration.[13]

On the other hand, the contribution of plasma oscillation to the $A_1(LO)$ and $E_1(LO)$ phonons was not reported in the Raman spectra.[11] Few attempts have been made to explain why the $A_1(LO)$ mode does not have a Fröhlich interaction with the plasma oscillation.[10,12] The coupling with the $E_1(LO)$ phonon observed by infrared measurements was also not clear.[13–15] This is due to the fact that when the carrier concentration decreases, the electron effective mass becomes smaller and the plasma frequency is close to or even smaller than 1000 cm^{-1}, and accordingly the reflection from the substrate obscures the coupling.

One of the best methods to make clear the strength of the Fröhlich interaction in InN is to investigate the phonon spectra as a function of carrier concentration. Recently Higashiwaki *et al*. succeeded in growing high quality InN with a low carrier concentration (2×10^{18} cm^{-3}) and high electron mobility (1500 $cm^2\,V^{-1}\,s^{-1}$) using a low-temperature-GaN/low-temperature-InN composite buffer structure on sapphire (0001).[16] In this study we used this buffer structure to grow Si-doped InN, and were able to vary the carrier concentration from 1.8×10^{18} to 1.5×10^{19} cm^{-3} without deteriorating the crystal quality. The infrared reflection spectra obtained at a normal incident configuration reveal the electron phonon interaction between the $E_1(LO)$ phonon and the plasma oscillation of free carriers. The Raman spectra obtained at backscattering configuration reveal the non-linear coupling between the $A_1(LO)$ phonon and the free carriers. With the

results of these studies, the electron effective mass of intrinsic InN and the anisotropy of the electronic structure of InN are discussed.

II. EXPERIMENTAL PROCEDURE

The samples were grown on sapphire (0001) by plasma-assisted MBE. Nitrogen radicals were supplied by a rf plasma cell. The MBE growth started with a thermal cleaning and nitridation of the sapphire substrate at 850 °C for 30 min. 10-nm-thick low temperature GaN and 10-nm-thick low temperature InN layers were grown sequentially at 380 °C. After that a 250-nm-thick InN layer was grown at 480 °C. Si doping was done in order to change the carrier concentration. The doping concentration was controlled by the evaporation temperature of the Si-effusion cell from 1120 to 1340 °C. The obtained InN had a carrier concentration (n_e) from 1.8×10^{18} to 1.5×10^{19} cm^{-3} and a mobility (μ_e) from 1000 to 1600 $cm^2\,V^{-1}\,s^{-1}$. The maximum mobility was obtained at a carrier concentration of 3.0×10^{18} cm^{-3}.

High resolution x-ray diffraction and reciprocal space mapping were performed in a Philips high resolution diffractometer with Cu $K\alpha_1$ radiation. No tetragonal metal In phase was detected. All of the samples investigated had metallic conduction and they did not show any resistivity anomaly at temperatures above 0.5 K. Infrared spectra were measured in a normal reflection configuration with a resolution of 1 cm^{-1} at room temperature. The Raman spectra ware taken at two excitation wavelengths of 488 and 633 nm using a combination of charge-coupled device detector and a single-path monochrometer with notch filters. The resolution of the Raman measurement was 1 cm^{-1} throughout the experiments.

III. RESULTS

A. Fourier transform infrared measurements

All of the InN films investigated had a hexagonal structure and their c axes were perpendicular to the sapphire (0001) planes. The lattice constants of InN were determined using four nonsymmetric reflections with large diffraction angles, and we obtained 3.53(2) Å for the a axis and 5.70(4) Å for the c axis as averages for the investigated samples. These values were much smaller than those reported by Tansley *et al.* ($a=3.548$ Å, $c=5.760$ Å),[3] whose samples were prepared by sputtering methods. The orientation of InN$[1\bar{2}10]$ was parallel to $Al_2O_3[10\bar{1}0]$.

In order to evaluate the crystal quality of InN investigated here, we measured absorption and photoluminescence spectra of pure InN, which are shown in Fig. 1. The absorption spectrum was obtained using a 1-μm-thick freestanding InN film. The film was fixed on an optically flat KRS-5 substrate. As reported before,[17] the low temperature InN buffer layer did not stick firmly to the GaN/sapphire substrate. Hence the 1-μm-thick InN film peeled off smoothly from the substrate, which let us determine the absorption coefficient without any optically complex contribution from the sapphire substrate. The square of the absorption coefficient had a linear dependence on the photon energy, as expected for a direct-band-gap semiconductor. The band gap energy is estimated to be 0.64–0.67 eV. The photoluminescence spectrum was obtained by the use of a combination of Yttrium aluminum garnet laser (1.06 μm) and an InSb photocell which had sensitivity from 0.4 to 1.1 eV. The luminescence was Lorentzian with the peak energy of 0.64 eV and the full width at half maximum (FWHM) of 0.1 eV. The peak position of the luminescence coincided with the band gap energy obtained at room temperature by the absorption measurement. These results are essentially the same as those reported before,[5,18] but the band gap energy obtained here is the smallest.

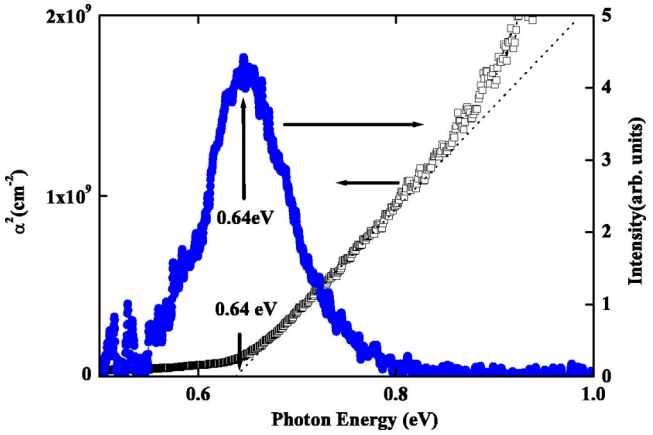

FIG. 1. Square of the absorption coefficient of nondoped InN together with the photoluminescence spectrum. The measurements were done at room temperatures.

It was reported that InN had strong plasma reflection for E$\perp c$ axis and that effective mass $m^*_{e\perp}$ of InN depended strongly on carrier concentration.[13] The analysis was based on Drude model where the carrier concentration was larger than 5.5×10^{18} cm^{-3}. As will be explained later, when the carrier concentration is in the order of 10^{19} cm^{-3}, we have to take into account the coupling between the plasma oscillation and the E_1(LO) phonon.[12,14] When the carrier concentration is at the order of 10^{18} cm^{-3}, we have to consider the contribution of the infrared-active optical phonons of the substrate sapphire for the determination of the plasma frequency.

Figure 2 shows the reflectivity spectrum of nondoped InN(250 nm)/buffer layers(20 nm)/sapphire at E$\perp c$ axis. The inset shows the reflectivity of the substrate sapphire (0001) at E$\perp c$ axis. In the spectrum there is a sharp reflectivity minimum at 460 cm^{-1}, and a structure due to plasma oscillation is observed at 550 cm^{-1}. When the carrier concentration increases, the reflection minimum shifts several cm^{-1} toward the higher energy side and the structure around 550 cm^{-1} becomes deeper. As seen in the inset of Fig. 2, the infrared active phonons of sapphire are so dominant that we have to consider the refractive index of sapphire for a determination of the plasma frequency of InN.

For the analysis of the optical reflectivity of InN, a stacking structure of air/InN/Al_2O_3 is taken into account. Here we treat the simplest case of normal incidence in the principal direction. From normal incidence, all wavevectors involved in the problem are collinear. In this case the boundary conditions for the incident light are given as follows:[19]

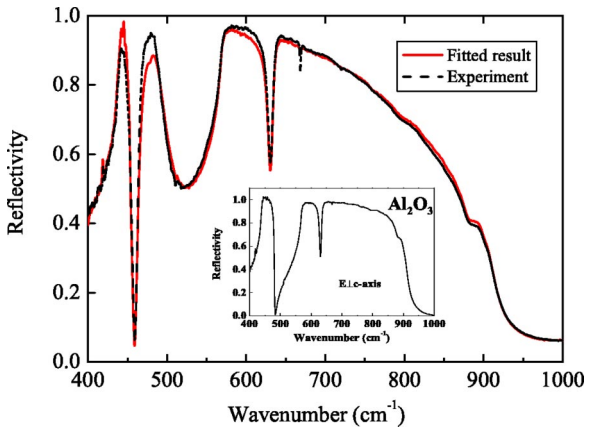

FIG. 2. Reflection spectrum of nondoped InN on sapphire at E⊥ c axis. The solid line is obtained by Eq. (6) with several fitting parameters given in the text. The inset shows the reflection spectrum of substrate sapphire on the (0001) surface.

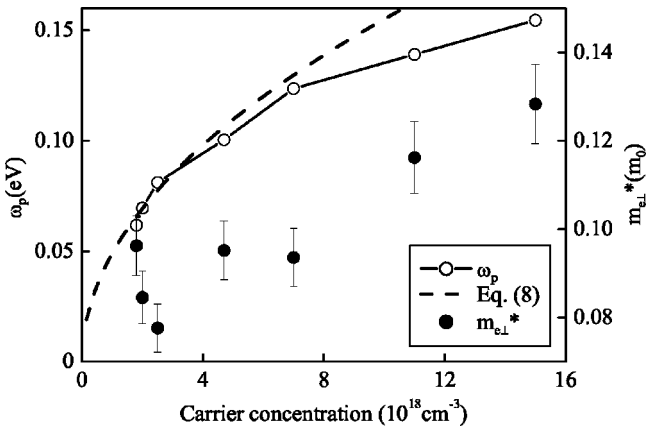

FIG. 3. Plasma frequency of InN as a function of the carrier concentration together with the effective electron mass. The dashed line is drawn from Eq. (8) using $m^*_{e\perp}=0.085m_0$ and $\epsilon_{\infty\perp}=6.7$.

$$E_{0i}+E_{0r}=E_{1i}+E_{1r}, \tag{1}$$

$$n_0(E_{0i}-E_{0r})=\hat{n}_1(E_{1i}-E_{1r}), \tag{2}$$

$$E_{1i}e^{ik\hat{n}_1 d}+E_{1r}e^{-ik\hat{n}_1 d}=E_2, \tag{3}$$

$$\hat{n}_1(E_{1i}e^{ik\hat{n}_1 d}-E_{1r}e^{-ik\hat{n}_1 d})=\hat{n}_2 E_2, \tag{4}$$

where, suffixes i and r represent incident and reflected waves, respectively. The suffixes 0, 1 and 2 are for air, InN and sapphire, respectively. d is the film thickness of InN, and k is the wave vector of radiation. From these equations, we obtain the reflectivity R of InN as follows:

$$R=\left|\frac{E_{0r}}{E_{0i}}\right|^2 \tag{5}$$

and

$$\frac{E_{0r}}{E_{0i}}=\frac{(\hat{n}_1-\hat{n}_2)(\hat{n}_1+n_0)e^{ik\hat{n}_1 d}+(\hat{n}_2+\hat{n}_1)(n_0-\hat{n}_1)e^{-ik\hat{n}_1 d}}{(\hat{n}_2-\hat{n}_1)(\hat{n}_1-n_0)e^{ik\hat{n}_1 d}+(\hat{n}_2+\hat{n}_1)(\hat{n}_1+n_0)e^{-ik\hat{n}_1 d}}. \tag{6}$$

In this equation, $\hat{n}_2$ is the refractive index of sapphire and is obtained from the reflectivity spectrum of sapphire using Kramers-Kronig relations. $\hat{n}_1$ is assumed to be the linear combination of the dielectric functions of free carriers (Drude model) and the E_1 infrared active mode of InN;

$$\hat{n}_1^2=\epsilon_{\infty\perp}\left(1-\frac{\omega_p^2}{\omega(\omega+i\gamma)}\right)+\frac{(\epsilon_{0\perp}-\epsilon_{\infty\perp})\omega_{TO}^2}{\omega_{TO}^2-i\Gamma\omega-\omega^2}. \tag{7}$$

Here, $\epsilon_{\infty\perp}$ and $\epsilon_{0\perp}$ are the high and low frequency dielectric constants of InN in the a-b plane, respectively. ω_p is the plasma frequency, γ is the damping factor of the plasma oscillation, ω_{TO} is the frequency of E_1(TO), and Γ is the damping factor of E_1(TO). For the fitting procedure, the film thickness d is dominant for the determination of the reflection minimum at 460 cm^{-1}. The best result is obtained at $d=280$ nm, which is in good agreement with the total film thickness of the 250-nm InN film and the 20-nm low-temperature GaN/InN buffer.

As seen in Fig. 2, the reflection spectrum is well reproduced by Eq. (6). The parameters determined for the best fitting are $\epsilon_{\infty\perp}=6.7$, which is the same as that reported before,[12] and $\epsilon_{0\perp}=10.5$. From the Lyddane-Sachs-Teller relation, $\omega_{LO}=600$ cm^{-1} is obtained for E_1 mode. $\omega_p=0.062$ eV, $\gamma=0.034$ eV, $\omega_{TO}=479$ cm^{-1}, and $\Gamma=4.8$ cm^{-1}. These frequencies of E_1 agree well with those reported before.[11] The small energy of Γ indicates that the lattice vibration in the a-b plane has a long lifetime and supports the good crystal quality. γ gives the optical mobility in the a-b plane of 430 cm^2 V^{-1} s^{-1} from $\gamma=e/\mu_e m^*_{e\perp}$, which is almost one-third of that obtained from Hall measurement.

The reflectivity spectra of other samples with different n_e are well reproduced using Eq. (6) without changing the fitting parameters except ω_p and γ. That is, the total reflectivity, which is determined by $\epsilon_{\infty\perp}$, does not depend on n_e. The deep reflection minimum observed around 460 cm^{-1} shifts to 467 cm^{-1} at the largest n_e, but the FWHM and the depth do not depend on n_e, which indicates that Γ and d are constants. This result indicates that Si doping does not change the E_1 phonon structure. $\epsilon_{0\perp}=10.5$ is satisfied in all of the investigated samples. ω_p and γ depend on n_e, and the obtained ω_p is plotted in Fig. 3 as a function of n_e. The square of ω_p does not depend linearly on n_e. Using n_e, the electron effective mass ($m^*_{e\perp}$) is given as follows:

$$\omega_p^2=\frac{n_e e^2}{\epsilon_{\infty\perp}m^*_{e\perp}}. \tag{8}$$

The carrier concentration dependence of $m^*_{e\perp}$ is also plotted in Fig. 3. The effective mass is nonlinear, as reported before,[13] but the value is stabilized around $0.085m_0$ at $n_e<8\times10^{18}$cm^{-3}. The error bars of $m^*_{e\perp}$ in Fig. 3 are due to the uncertainty of n_e determined by Hall measurements ($\pm5\%$). As shown in Fig. 3, ω_p is fitted well by Eq. (8) of $m^*_{e\perp}=0.085m_0$. We therefore conclude that pure InN has an

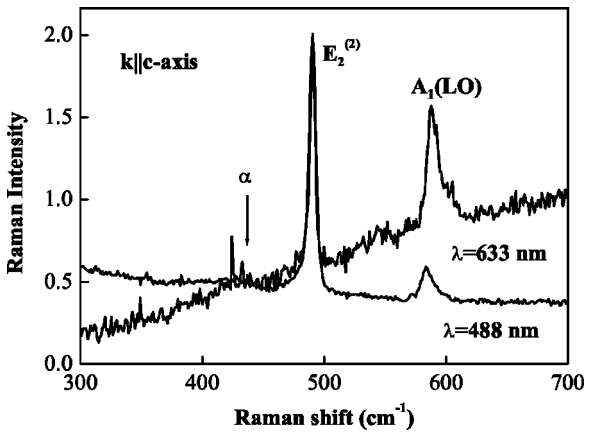

FIG. 4. Comparison of the micro-Raman spectra of nondoped InN observed by 488-nm excitation and 633-nm excitation. The Raman spectra were taken at a backscattering configuration where the wave vector of the laser was parallel to the crystal *c* axis.

$m_{e\perp}^*$ of $0.085m_0$. At $n_e > 8\times10^{18}$ cm^{-3}, ω_p deviates from Eq. (8), which might be due to the nonparabolicity of the conduction band originated from the $k\cdot p$ interaction between the conduction and valence bands as is observed in narrow band gap semiconductors.[20]

The fitted γ becomes small with increasing n_e and reaches a minimum at $n_e = 4.7\times10^{18}$ cm^{-3}, where $\gamma = 0.014$ eV, which gives $\mu_e = 1240$ cm^2 V^{-1} s^{-1}. This is very close to the 1500 cm^2 V^{-1} s^{-1} obtained by Hall measurement at room temperature.

B. Raman scattering measurements

The micro-Raman spectra of InN have a strong excitation energy dependence. In Fig. 4 we compare the Raman spectra of nondoped InN obtained by 488- and 633-nm excitation energies. The laser direction is parallel to the hexagonal *c* axis and the Raman spectra are observed in a backscattering configuration. In this configuration the following three modes are Raman active. One is the strong $E_2^{(2)}$ mode at 490 cm^{-1}. The FWHM of this mode is 4 cm^{-1}. The position and FWHM of this mode do not show an excitation energy dependence. Hence Fig. 4 is drawn so as to fix the $E_2^{(2)}$ peaks at the same intensity. The second is the $E_2^{(1)}$ mode at 87 cm^{-1} (not shown in the figure). The third is the A_1(LO) which is expected to be observed at around 590 cm^{-1} from an *ab initio* calculation.[21] As seen in Fig. 2, nondoped InN has $\omega_p = 500$ cm^{-1}, and therefore the A_1(LO) mode should couple with free carriers linearly and be observed as plasmon–LO-phonon coupled (PLP) modes. Assuming spherical electron mass, PLP$^-$ and PLP$^+$ (lower and upper plasmon–LO-phonon coupled modes) should be observed at 310 and 700 cm^{-1}, respectively. Since we could not observe any intensity around there as is shown in Fig. 4, we assign the peak around 590 cm^{-1} as A_1(LO). Under 488-nm excitation the peak is observed at 583 cm^{-1}. This peak shifts to 586 cm^{-1} under 633-nm excitation. The shape of A_1(LO) is asymmetric, and the FWHM is 10 cm^{-1}. There is another weak band around 433 cm^{-1}, which is denoted by α in Fig. 4.

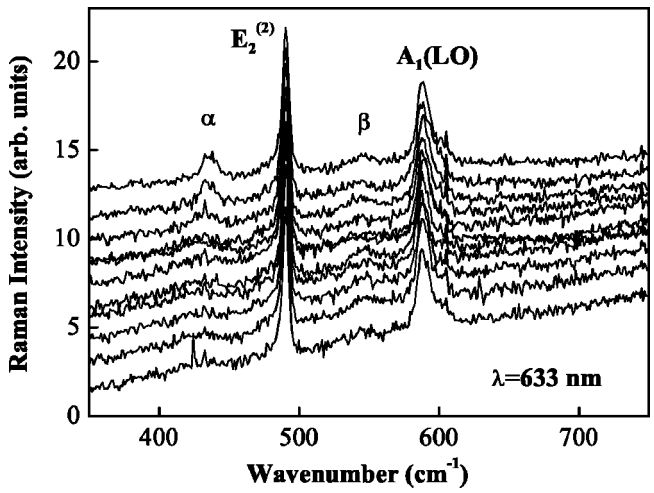

FIG. 5. Sample dependence of the Raman spectra of InN excited by 633 nm. n_e(cm^{-3}) and μ_e(cm^2 V^{-1} s^{-1}) of the samples shown in the spectra are, from bottom to top, 1.8×10^{18}, 1280 (nondoped); 2.2×10^{18}, 1390; 2.2×10^{18}, 1520; 2.5×10^{18}, 1570; 3.0×10^{18}, 1600; 3.7×10^{18}, 1490; 4.7×10^{18}, 1500; 7.0×10^{18}, 1340; 7.6×10^{18}, 1280; 1.1×10^{19}, 1020; and 1.5×10^{19}, 1000.

There is another remarkable change in the Raman spectrum when the excitation energy changes from 488 nm to 633 nm. The Raman intensity of A_1(LO) obtained by 633-nm excitation is four times stronger than that by 488 nm. The background with positive slope with the Raman shift, which increases up to 1200 cm^{-1}, becomes dominant at 633-nm excitation. The big change of the Raman spectrum should be due to the resonance Raman effect because $\lambda = 633$ nm is closer to the band gap energy of InN.

Figure 5 shows the carrier concentration dependence of the micro-Raman spectra obtained by 633-nm excitation. In this figure each Raman spectrum is obtained under the same experimental condition and is plotted on the same scale. The dark noise was subtracted systematically. The Raman spectrum consists of two components: a discrete structure due to Raman active phonons and a linearly increasing background with positive slope against the Raman shift. The background intensity increases as n_e increases, while the slope of the background becomes less steep. The background part of the Raman intensity should originate from the free carriers of InN.

As for the discrete structure, there is little n_e dependence, which indicates that the crystal quality is kept almost constant against Si doping. The peak position and FWHM of the $E_2^{(2)}$ phonon do not show any n_e dependence. The n_e dependence of the frequency of the A_1(LO) mode is small, but it is not impossible to evaluate the shift from 586 to 589 cm^{-1} as n_e changes. The mode denoted by α becomes a clear peak, but its position is almost constant against the increase of n_e.

Davydov *et al.* assigned the origin of peak α as PLP$^-$ using Mg-doped InN.[11] As shown in Fig. 5, the n_e dependence of the Raman shift of peak α is negligible, which reveals that the origin of α is not PLP$^-$. Kasic *et al.* assigned this peak as a disorder-activated A_1(TO) peak, and determined its energy to be 443 cm^{-1}.[12] Their assignment is based on the FWHM of peak α, which is much wider than

that of $E_2^{(2)}$. In Fig. 5, the FWHM of peak α is 10 cm^{-1}, similar to that of $A_1(LO)$. Moreover the line shape of peak α is asymmetric like $A_1(LO)$, which indicates that the physical origin of peak α is similar to that of $A_1(LO)$.

To understand the mechanism of the appearance of $A_1(LO)$ under strong plasma reflection, one of the authors (T.I.) proposed the presence of an extended carrier-depleted layer at the sample surface.[10] Kasic *et al.* denied this by precise infrared spectroscopic ellipsometry measurements.[12] They assigned the $A_1(LO)$ peak as the lower branch of the large-wave-vector LO-phonon-plasmon coupled mode [the PLP^- mode approached $A_1(LO)$] arising through a nonconservative wave-vector scattering process. Their assignment was based on one sample of $n_e = 2.8\times10^{19}$ cm^{-3}. If we apply their mechanism to our data shown in Fig. 5, the peak denoted as $A_1(LO)$ has to show a strong n_e dependence, because in small n_e samples ω_p is much smaller than the frequency of $A_1(LO)$. The data shown in Fig. 5 do not support their assignment. We will discuss the origin of $A_1(LO)$ together with peak α in Sec. IV. A peak, denoted by β in Fig. 5, becomes observable at 550 cm^{-1} with the increase of n_e. At present we cannot assign the origin of this peak. Davydov *et al.*[11] and Kasic *et al.*[12] reported a peak at around 561 cm^{-1}. The relationship between these two peaks is not clear.

IV. DISCUSSION

Germanium and Si are nonpolar materials and their optical phonons at $k=0$ are not infrared active. Consequently they do not split at $k=0$ into LO and TO components. There is no Fröhlich scattering mechanism, or LO-phonon–plasmon coupled mode. In these nonpolar semiconductors the interaction between free carriers and phonons is nonlinear and optical phonons are observed as Fano interference, showing an asymmetric shape at the initial positions. On the other hand, in polar semiconductors, Fröhlich interaction is so strong that only plasmon–LO-phonon coupled modes are observed.[22] The results shown in Fig. 5 indicate that the LO phonons of InN observed around 590 cm^{-1} do not couple with free carriers. They have a strong excitation energy dependence, their peak positions shift a little as n_e changes, and they are shaped asymmetric at their original position. These features are essential to the Fano interference as is observed in nonpolar semiconductors.

Here we discuss the Raman spectra shown in Fig. 5 based on the Fano interference. As seen in Figs. 4 and 5, when the penetration depth of the irradiation or n_e increases, the Raman intensity increases, where the spectrum is linear with the Raman shift. This feature was observed in the Raman spectra of high-T_c superconductors[23] and the mechanism was explained by Zawadowski and Cardona.[24] According to them, the Raman intensity is dominated by the scattering between different parts of the Fermi surface of degenerate semiconductors. When the light produces pair excitations with different angular momentum quantum numbers L, the electron-density fluctuations with $L=0$, which corresponds to isotropic excitation, are screened by plasma oscillations and result in weak Raman intensity. The excitations with $L\neq0$ do not form plasma oscillations and they are free from long-range Coulomb forces, but they are coupled to optical phonons and Fano resonances are expected. The Raman intensity in the case of $L\neq0$ is determined by the scattering rate (τ_L^{-1}) in channel L and when $\tau_L^{-1} > \omega$, the Raman spectrum is linear in energy ω. Now, when the free electrons in InN spread in the *a-b* plane, they should have a strong interaction with the $A_1(LO)$ phonon because of the out-of-phase vibration of In and N atoms along the *c* axis in the unit cell. In this case the Raman intensity $S(\omega)$ is expressed with the combination of the Fano interference[25] and the contribution of channel $L\neq0$ as follows:

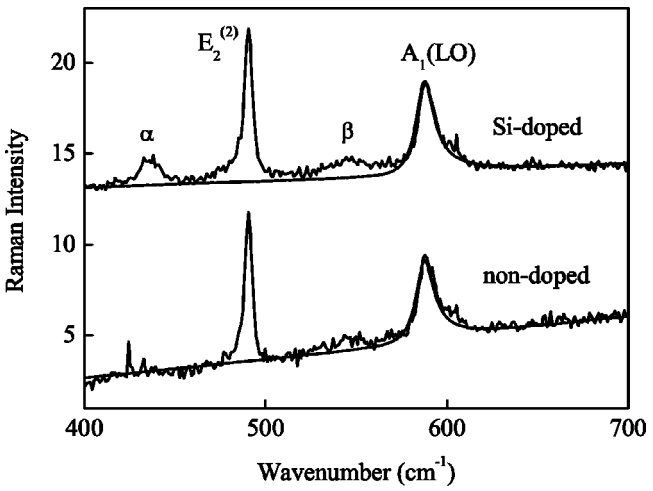

FIG. 6. Raman spectra of nondoped ($n_e = 1.8\times10^{18}$ cm^{-3}) and Si-doped ($n_e = 1.5\times10^{19}$ cm^{-3}) samples. The solid lines represent theoretical fits to the Fano profiles of Eq. (9).

$$S(\omega) \propto \frac{1}{1-e^{-\omega/kT}}\left[\frac{(q+\epsilon)^2}{1+\epsilon^2}+\omega\tau_L\right] \tag{9}$$

and

$$\epsilon = \frac{\omega-\omega_0-\Delta\omega}{\Gamma_F}, \tag{10}$$

where q is the Fano asymmetry parameter for the coupling of the phonon to the electronic continuum, ω_0 is the frequency of the $A_1(LO)$ phonon, $\Delta\omega$ is the shift of the phonon energy due to the electron-phonon interaction, and Γ_F is the width parameter related to the transition rate between the continuum and discrete states. τ_L determines the slope of the background spectrum.

The fittings of the Fano interference to the Raman spectra of the non-doped and the most heavily Si-doped InN are shown in Fig. 6. The fitting parameters are common to both spectra: $q=9$, $\omega_0 = 586$ cm^{-1}, $\Gamma_F = 6$ cm^{-1}, and $T = 400$ K. $\Delta\omega = 0$ for the nondoped InN and $\Delta\omega = 3$ cm^{-1} for the Si-doped InN. As for τ_L, we can reproduce the Raman spectra using $\tau_L = 0.3$ for the nondoped InN and $\tau_L = 0.18$ for the Si-doped InN. The factor τ_L is related to the transport lifetime, and becomes smaller when the impurity concentration increases. Hence Eq. (9) explains well the result of Fig. 5 that the Raman slope becomes less steep against the increase of n_e.

In the highly Si-doped InN, the Fano interference is also observed at peak α and the parameters q and Γ_F are similar to those obtained for the A_1(LO) mode. This fact indicates that peak α is an optical phonon with the same representation as that of A_1(LO). Hence we assign peak α as A_1(TO), though this mode is forbidden at this scattering configuration. It becomes observable at 433 cm^{-1} in the Raman spectra due to the increase of lattice imperfections in heavily Si-doped InN. As for the uncoupled A_1(TO) phonon energy, Davydov *et al.* reported it to be 447 cm^{-1} using InN grown on $(1\bar{1}02)$ sapphire.[11] Then we assign the most appropriate energies for A_1(TO) and A_1(LO) as 447 and 586 cm^{-1}, respectively. From Lyddane-Sachs-Teller relation $\epsilon_{0||}/\epsilon_{\infty||} = 1.72$, which is larger than $\epsilon_{0\perp}/\epsilon_{\infty\perp} = 1.57$.

Next we consider why InN has a strong nonlinear free-carrier–LO-phonon interaction rather than Fröhlich interaction along the *c* axis, or why the excitations with $L \neq 0$ are dominant in InN. The most plausible explanation is the anisotropic electronic structure of InN. This structure was observed in InN by the magnetoresistance measurements, and was reported before.[8,9] If the anisotropy is strong along the *c* axis, the coupling between the electrons moving along the *c* axis becomes incoherent. Consequently, the charge density fluctuations are not followed by long-range Coulomb fields, and the phonon polarization field is not screened by free carriers. Instead, a broad continuum of free carrier excitation appears along the *c* axis. In this case Fano type coupling between the electron-excitation continuum and the LO phonon takes place when the excitation energy of the electron in the continuum overlaps with that of the LO phonon. The experimental conditions required to observe the Fano-type coupling can be easily fulfilled in InN because the electronic states are uniformly spread in the *a*-*b* plane, as shown in Fig. 2, while there are many stacking faults in InN, as shown in the broad luminescence in Fig. 1, which should be along the *c* axis.

There are several reports that the Fano interferences are observed in polar semiconductors. In contrast to homogeneously doped GaAs, where LO-phonon–plasmon coupled modes are observed, a strong Fano interference is dominant in a periodically delta-doped multilayer-structure of GaAs.[26] In such a system, electron motion in the direction normal to the doped layers is quantized in the form of minibands and hence the Fano-like interferences between electronic minibands and the LO phonon were reported.

V. CONCLUSION

In this paper we present the carrier concentration dependence of the interaction between free carriers and LO phonons of InN, studied by Raman scattering and Fourier transform infrared measurements. The infrared reflection spectra reveal linear-coupling between the E_1(LO) phonon and the plasma oscillation of the free carriers. The obtained phonon energies for E_1(TO) and E_1(LO) phonons are 479 and 600 cm^{-1}, respectively. From the plasma frequency the electron effective mass is estimated to be $m^*_{e\perp} = 0.085\ m_0$ for the intrinsic InN. The Raman spectra reveal that the A_1(LO) phonon and free carriers couple nonlinearly and the Fano interferences are prominent between the zone-center LO phonon and a quasicontinuum electronic state along the *c* axis. From these results, we decide that the most appropriate energies for A_1(TO) and A_1(LO) are 447 and 586 cm^{-1}, respectively. From these considerations, we propose an anisotropic electronic structure of InN.

ACKNOWLEDGMENTS

The authors are grateful to Professor H. Harima of Kyoto Institute of Technology for his advice, to the Ministry of Education for the Grant-in-Aid for Scientific Research (C)14550306 and to the financial support of the Nippon Sheet Glass Foundation. The low temperature measurement was carried out at the High Field Laboratory for Superconducting Materials of Tohoku University. We also appreciate the support of Dr. Ohkubo of Jasco Corporation and Mr. Chihaya of Atago Bussan Co., Ltd.

*Email address: inushima@keyaki.cc.u-tokai.ac.jp

[1] S. Nakamura and F. Fasol, *Blue Laser Diode* (Springer-Verlag, Berlin, 1997).
[2] K. Osamura, K. Nakajima, Y. Murakami, P.H. Shingu, and A. Ohtsuki, Solid State Commun. **11**, 617 (1972).
[3] T.L. Tansley and C.P. Foley, J. Appl. Phys. **59**, 3241 (1986).
[4] T. Inushima, V.V. Mamutin, V.A. Vekshin, S.V. Ivanov, T. Sakon, S. Motokawa, and S. Ohoya, J. Cryst. Growth **227-228**, 481 (2001).
[5] V.Y. Davydov *et al.*, Phys. Status Solidi B **229**, R1 (2002).
[6] V.Y. Davydov *et al.*, Phys. Status Solidi B **230**, R4 (2002).
[7] B.R. Nag, Phys. Status Solidi B **233**, R8 (2002).
[8] T. Inushima, V.V. Mamutin, V.A. Vekshin, S.V. Ivanov, V.V. Davydov, T. Sakon, and M. Motokawa, Phys. Status Solidi B **228**, 9 (2001).
[9] T. Inushima, T. Takenobu, M. Motokawa, K. Koide, A. Hashimoto, A. Yamamoto, Y. Saito, T. Yamaguchi, and Y. Nanishi, Phys. Status. Solidi C **0**, 364 (2002).
[10] T. Inushima, T. Shiraishi, and V.Y. Davydov, Solid State Commun. **110**, 491 (1999).
[11] V.Y. Davydov, V.V. Emtsuev, I.N. Goncharuk, A.N. Smirnov, V.D. Petrikov, V.V. Mamutin, V.A. Vekshin, S.V. Ivanov, M.B. Smirnov, and T. Inushima, Appl. Phys. Lett. **75**, 3297 (1999).
[12] A. Kasic, M. Schubert, Y. Saito, Y. Nanishi, and G. Wagner, Phys. Rev. B **65**, 115206 (2002).
[13] J. Wu, W. Walukiewicz, W. Shan, K.M. Yu, J.W. Ager III, E.E. Haller, H. Lu, and W.J. Schaff, Phys. Rev. B **66**, 201403 (2002).
[14] T. Inushima, T. Takenobu, M. Motokawa, K. Koide, A. Hashimoto, A. Yamamoto, Y. Saito, T. Yamaguchi, and Y. Nanishi, Physik Mikrostrukturierter Halbleiter **27**, 131 (2002).
[15] Z.G. Qian, G. Yu, W.Z. Shen, H. Ogawa, and Q.X. Guo, Physica B **318**, 180 (2002).
[16] M. Higashiwaki and T. Matsui, Jpn. J. Appl. Phys. **41**, L540 (2002).
[17] M. Higashiwaki and T. Matsui, J. Cryst. Growth **251**, 494 (2003).
[18] T. Matsuoka, H. Okamoto, M. Nakao, H. Harima, and E.

Kurimoto, Appl. Phys. Lett. **81**, 1246 (2002).
[19] A.S. Barker, Jr. and M. Ilegems, Phys. Rev. B **7**, 743 (1973).
[20] E.O. Kane, J. Phys. Chem. Solids **1**, 249 (1957).
[21] C. Bungaro, K. Rapcewicz, and J. Bernholc, Phys. Rev. B **61**, 6720 (2000).
[22] G. Abstreiter, M. Cardona, and A. Pinczuk, *Light Scattering in Solids IV*, Topics in Applied Physics, Vol. 54 (Springer-Verlag, Berlin, 1984), p. 5.
[23] S.L. Cooper, F. Slakey, M.V. Klein, J.P. Rice, E.D. Bukowski, and D.M. Ginsberg, Phys. Rev. B **38**, 11 934 (1988).
[24] A. Zawadowski and M. Cardona, Phys. Rev. B **42**, 10 732 (1990).
[25] U. Fano, Phys. Rev. **124**, 1866 (1961).
[26] L.A.O. Nunes, L. Ioriatti, L.T. Florez, and J.P. Harbison, Phys. Rev. B **47**, 13 011 (1993).